ChemPubSoc Europe

DOI: 10.1002/batt.201800109

BATTERIES & SUPERCAPS
Articles

Special Issue

A Comparison of Formation Methods for Graphite//$LiFePO_4$ Cells

Arianna Moretti,*[a, b] Varvara Sharova,[a, b] Diogo V. Carvalho,[a, b] Adrien Boulineau,[c] Willy Porcher,[c] Iratxe de Meatza,[d] and Stefano Passerini*[a, b]

The sequence of initial cycles necessary for the build-up of the solid electrolyte interphase (SEI) on the anode surface of Li-ion batteries (usually called formation) is a cost- and time-consuming process, thus requiring further optimization. Herein, three different protocols are compared to explore possibilities to reduce the formation time of the cells without negatively affecting the electrochemical performance. XPS and HRTEM analyses are used to identify the main characteristics of the as formed SEIs. Electrochemical tests are conducted on full lithium-ion cells using state-of-the-art graphite and $LiFePO_4$ electrodes. The time-saving dual-current protocol results in excellent cycling performance, and in a LiF-rich SEI. Interestingly, the use of moderately high temperature (40 °C) does not strongly affect the SEI composition as evidenced by XPS analysis. On the other hand, the formation rate determines the degree of graphite surface amorphization, visualized by HRTEM.

1. Introduction

The depletion of fossil fuels and the severe air pollution and climate change caused by their combustion, is leading the society towards the use of renewable energy sources, such as wind, solar or hydropower. These sources are, however, discontinuous in time and geographical distribution, thus requiring appropriate storage technologies. Rechargeable lithium-ion batteries (LIBs) are suitable energy storage systems that reversibly convert chemical energy into electricity with high energy efficiency, on demand. LIBs can also supply energy to an electric motor for vehicles propulsion, enabling reduced polluting emissions or even the complete removal of the internal combustion engine.

Commercial LIBs use graphite as negative electrode. The reversible insertion of Li ions in the graphite structure occurs at voltages close to that of metallic lithium (−3.04 V *vs* SHE). However, below 1 V (*vs* Li/Li^+), the state-of-the-art electrolytes (i.e., solutions of lithium hexafluorophosphate ($LiPF_6$) in mixed organic carbonates) are unstable. Indeed, mainly during the first charge, the electrolyte undergoes reductive decomposition at the anode surface with the formation of a passivation film known as the solid electrolyte interface (SEI).[1] The SEI plays a central role in ensuring the reversibility of the Li^+ intercalation/de-intercalation process in the following cycles. Being an electronic insulator, but at the same time allowing the Li^+ transport across the anode surface, the SEI prevents the continuous electrolyte decomposition, which would result in the unlimited growth of the passivation layer causing the rapid capacity decay of the cell. However, the SEI formation during the initial cycles requires the irreversible consumption of a fraction of the lithium ions reservoir, i.e., depleting the cathode capacity. The most widely accepted model describes the SEI being composed of multiple layers.[2] The inner one, i.e., the one in contact with the anode surface, is rich in insoluble inorganic compounds (e.g., LiF, Li_2CO_3, Li_2O), while the outer one is predominantly composed of less stable organic and polymeric compounds, such as $ROCO_2Li$, ROLi and polycarbonates.[3] However, the actual cross-sectional distribution of components, the composition and thickness of the layers vary, substantially depending on the anode surface, the electrolyte formulation and the conditions used for the formation process, such as, e.g., temperature and current density. The low thickness and high reactivity towards air and moisture of the SEI (requiring special sample handling and experimental set-up) limit the number of techniques that can be used to disclose its complex nature.

The series of initial charge/discharge cycles and rest periods necessary to generate a stable and uniform SEI is, as a whole, usually called "cell formation". This process represents an industrial bottleneck, as it requires specific instrumentation and a large area of the battery production plant, significantly influencing the manufacturing costs of LIBs (up to 30 $/kWh of the total cell cost, according to[4]). Furthermore, the cell formation can take from 4–5 days up to a few weeks including monitored aging at open circuit voltage (OCV),[5] resulting in additional energy consumption and further capital costs. There-

[a] Dr. A. Moretti, Dr. V. Sharova, Dr. D. V. Carvalho, Dr. S. Passerini
Helmholtz Institute Ulm (HIU)
Helmholtzstraße 11, 89081 Ulm, Germany
E-mail: arianna.moretti@kit.edu
stefano.passerini@kit.edu
[b] Dr. A. Moretti, Dr. V. Sharova, Dr. D. V. Carvalho, Dr. S. Passerini
Karlsruhe Institute of Technology (KIT)
PO Box 3640, 76021 Karlsruhe, Germany
[c] Dr. A. Boulineau, Dr. W. Porcher
CEA, LITEN
Rue des Martyrs, 17, 38054 Grenoble, France
[d] Dr. I. de Meatza
CIDETEC, Energy Storage
Paseo Miramon 196, 20014 Donostia-San Sebastián, Spain

Supporting information for this article is available on the WWW under https://doi.org/10.1002/batt.201800109

Special Issue *An invited contribution to a Special Issue on SEI and Interphases at Electrodes*

fore, accelerating the cell formation step is highly desirable. Unfortunately, battery manufacturers independently develop the most advantageous formation protocol, keeping the results confidential. This limits the amount of available literature to compare different protocols and evaluate the influence of the different parameters (e.g., current density, rest time, and temperature) on the SEI formation and cell capacity retention.

Formation methods proposed in the available literature include the constant current formation in one or two steps,[6] pulse formation[7] and elevated temperature aging,[8] often combined in a complex protocol. During the constant current formation, relatively low current densities, corresponding to C-rates between C/20 and C/5, are used since the resulting SEI offers higher ionic and lower electronic conductivity,[2] but at the expense of production costs associated with the longer formation times. When higher current densities are used, the SEI is formed faster, but it is generally more porous and electronically conductive, leading to the reduced cycle life of the cell.[2] Formation at elevated temperatures (~40 °C) results in the formation of a more compact SEI, rich in insoluble inorganic components on the surface of graphite.[8] A recently published study proposed a new formation protocol in which, after the complete charge, few discharge/charge cycles were performed within a high state of charge (SOC). This protocol resulted in reduced interfacial resistance, improved long-term cycling performance, and a 6-fold reduction of formation time.[9]

Herein, we compare three different formation protocols to evaluate their influence on the cell lifetime and on the characteristics of the corresponding SEIs formed on state-of-the-art graphite electrodes. Full cells were assembled using a $LiFePO_4$ (LFP) cathode to simulate the condition in real cells, thus eliminating the electrolyte degradation at the lithium metal interface, but evidencing the Li^+ inventory loss issue. The easiest of the three protocols (called "single-current") is often used in materials research laboratories and involves a single constant current (CC) step. The second protocol (designated as "dual-current") involves two CC steps at different rates aiming at reducing the formation time. Finally, a more articulated protocol (called "advanced"), obtained from a graphite//LFP battery manufacturer, is used as a model for the actual industrial processes. It included a pre-charge and a long rest time, and it is partially conducted at 40 °C. X-ray photoelectron spectroscopy (XPS), and high resolution transmission electron microscopy (HRTEM) are used to derive detailed information on the main features of the SEI formed on graphite electrodes.

2. Results and Discussion

2.1. Formation Protocols Applied to Graphite//LFP Cells

Three formation protocols, reported in Table 1, are compared using graphite//$LiFePO_4$ coin cells, thus fixing the Li inventory (determined by the amount of $LiFePO_4$). Figure 1a and Figure 1b report the voltage and current profiles of such cells during the first charge/discharge cycle. The single-current protocol resembles the one most frequently used in academic laboratories. Generally, it is performed at low rate, herein at C/20, to ensure the homogeneous SEI formation,[6,7b] but the long time required does not make it appealing for battery manufacturers.

Table 1. Description of the three formation protocols compared in this work. A constant voltage (CV) step is applied at the end of the charge until the current decreases to a specific value of C or for 1 hour.

Formation protocol	Step	Conditions	Total duration[*]
Single-current	*Charge*	*C/20→3.6 V CV < C/20 or 1 h*	32 h
	Discharge	C/20→2.5 V	
Dual-current	*Charge*	*C/20→3 h C/10→3.6 V CV < C/20 or 1 h*	18 h
	Discharge	C/10→2.5 V	
Advanced	Pre-charge	At 20 °C: C/10→3.0 V	28 h
	Rest	At 40 °C: 10 h	
	Charge	*At 40 °C: C/10→3.6 V CV < C/100*	
	Rest	At 40 °C: 30 min	
	Discharge	At 40 °C: C/10→2.5 V	
	Rest	At 20 °C: 1 h	

[*]The initial wetting, which was the same for all formation protocols and comprised 24 h, is not included in the total time.

The dual-current protocol consists in a constant current charging at C/20 till the complete formation of the SEI occurs. This is considered achieved when the graphite electrode reaches the potential of 0.2 V vs Li/Li^+.[2–3,10] Therefore, a test in three-electrode cell, using Li metal as reference, was conducted to determine the time necessary to reach the complete SEI formation (see Figure S1 in the Supporting information). After, the cell was charged up to 3.6 V at C/10 and the same C-rate was used for the subsequent de-lithiation. This protocol allows a substantial time saving compared to the others as can be seen in Table 1.

In the third examined protocol, designated as "advanced" (see Table 1), the cell was initially pre-charged up to ~3.0 V. This preliminary step is reported to ensure that the anode potential is below the threshold of Cu corrosion (~3.3 V *vs* Li/Li^+)[11] to prevent the current collector degradation during the long rest time (10 h) at 40 °C. However, it should be noted that during the rest time the cell voltage dropped down, thus in our conditions the current collector protection may not have been fully realized. Afterwards, the cell was charged in CC–CV mode at C/10, followed by the rest period (30 min) and discharged using the same C-rate.

In Figure 1c the voltage profiles are normalized by state of charge (SOC), i.e., including the constant voltage step at the end of the charge.

Due to the flat voltage of LFP, the three plateaus visible in the cell profile, indicated with I, II and III in Figure 1c, mirror those of the negative electrodes, resulting from the graphite stage transitions upon intercalation of Li^+. Below 10%SOC, which is the region where the SEI formation contributes most to the charge capacity, the curve of the advanced protocol

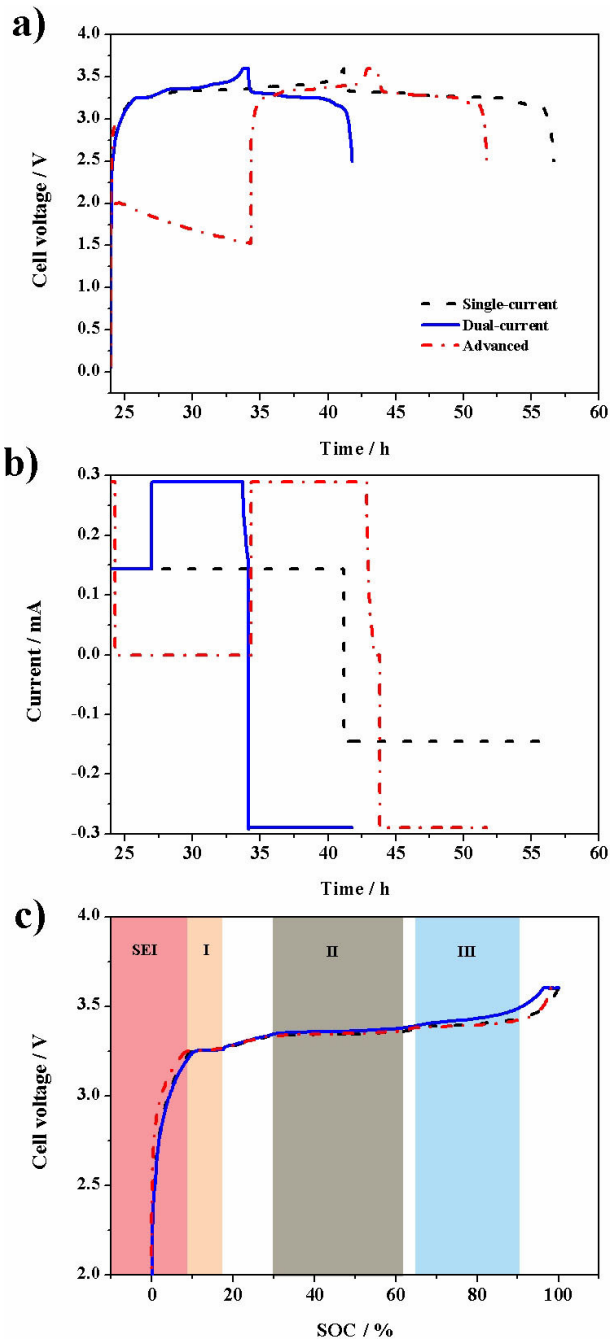

Figure 1. a) Voltage and b) current profiles recorded during the formation protocols described in Table 1. Note that in the advanced protocol only the pre-charge is conducted at 20 °C. c) Comparison of charge voltage profiles normalized by SOC. The curve is divided in four regions: below 10% SOC is the portion where the SEI formation contributes to the charge capacity, while I, II and II indicate the plateau due to graphite staging at different SOC.

differs slightly from the others, indicating that a reduced Li^+ consumption (i.e., reduced side reaction) occurs before the intercalation process takes place in spite of the higher temperature (40 °C).

The length of the first and second plateau are similar for all the cells, but the profile of the dual-current has a shorter third plateau, which corresponds to the last stage of the Li+ intercalation into graphite.

This observation most probably relates with the applied C-rate (twice that of the single current protocol) and temperature (lower than that of the advanced protocol). The subsequent discharge voltage profiles are reported in Figure S2 (Supporting Information) while the coulombic efficiencies (CE) are above 90% for all the protocols.

After formation the cells were subjected to rate tests (see Table S1 in the Supporting information), showing similar performance up to 3 C (Figure S3 in the Supporting information). The test continued with the evaluation of the battery lifetime at 1 C. The results, reported as the average of three cells for each formation protocol together with their standard deviation, are shown in Figure 2 (the results for each cell are reported in Figure S4 in the Supporting information).

All the cells retain more than 95% of their initial capacity over 400 cycles, in particular 97.2, 96.3 and 95.5% for single-, dual-current and advanced protocols, respectively.

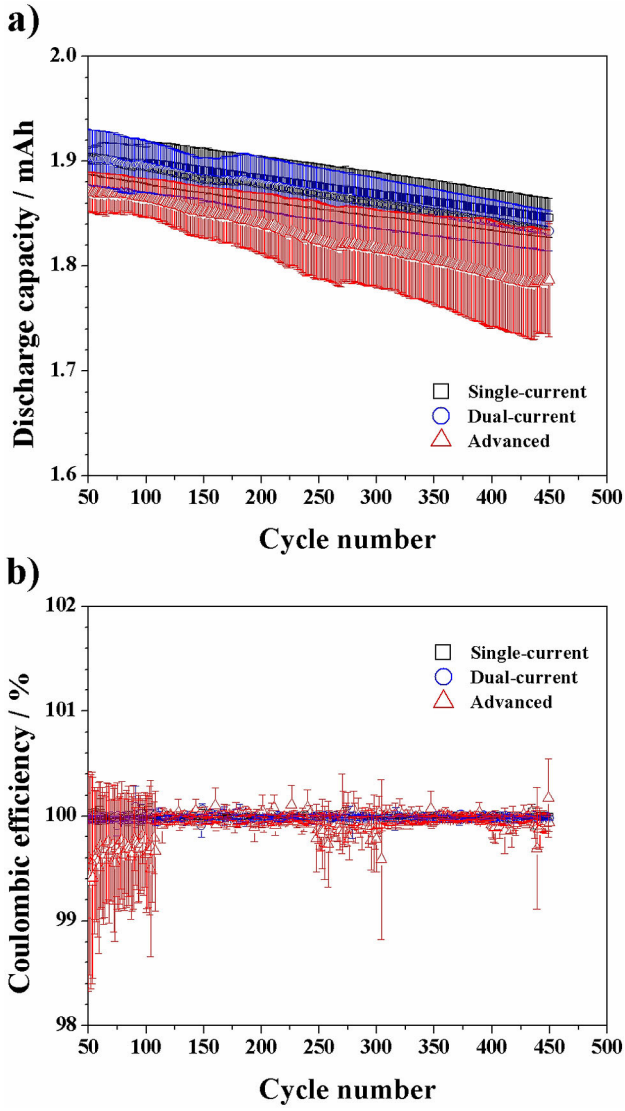

Figure 2. a) Average discharge capacity and b) average coulombic efficiency with relative standard deviation as error bars (obtained from three cells for each formation condition) during cycling at 1 C and 20 °C.

Despite the satisfactory performance, the cells that were formed using the advanced protocol showed faster capacity decay, lower coulombic efficiency and larger standard deviation than the others. These suggest the occurrence of uncontrolled side reactions during cycling, probably due to the non-optimal SEI formed with the advanced protocol and leading to larger fluctuations of the coulombic efficiency among the same group of cells and upon cycling.

A recent study based on graphite half-cells proposes a dual-current formation protocol inverse to ours, i.e., where the cells spend less time at higher potential (>240 mV).[7b] The graphite anodes displayed a better rate capability than those subjected to a standard formation at C/10, the formation of a more granular, open SEI with more efficient ion channels was proposed. The effect on the long-term cycling of full-cells (thus with limited Li reservoir) was not reported. However, our results (Figure 2) confirm the expectation that a slow SEI formation warrants long term cycling performance as no major differences are seen between the single- and dual-current protocols, with both cells showing excellent capacity retention and stable coulombic efficiency. However, additional experiments using full-cells and faster SEI formation steps are necessary to clarify whether the persistence of the anode at high voltage is necessary to achieve long cycle life of full-cells.

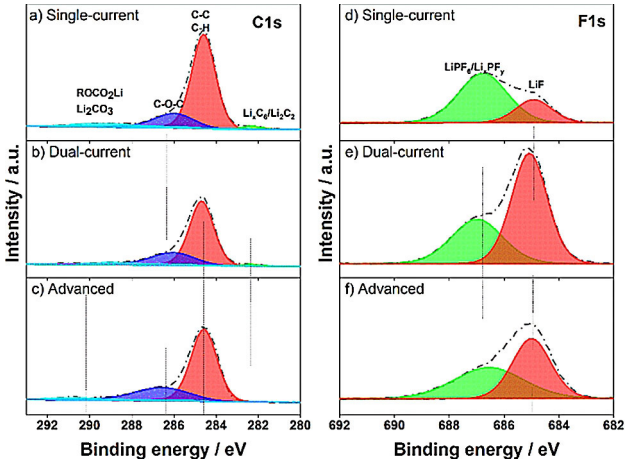

Figure 3. C1 s (a–c) and F1s (d–e) XPS spectra of graphite electrodes after different charging protocols.

2.2. Ex-Situ XPS Analysis of the Lithiated Graphite Electrodes

The XPS analysis of the SEI was conducted on charged (i.e., lithiated) graphite electrodes extracted from full-cells subjected to the different formation protocols.

Figure 3 shows the C1s and F1s spectra while Figure 4 reports the estimated atomic fraction for the species on the graphite surface. The O1s and P2p spectra are reported in Figure S4 in the Supporting information. From Figure 3a–c, it can be seen that for all the extracted electrodes the peak with the highest intensity is the one occurring at 284.6 eV, which corresponds to C–C and C–H groups[3] attributed mainly to the graphite and the binder. The detection of these peaks, belonging to the pristine electrode surface, supports for rather thin SEI layers covering the electrodes. The C–O–C peak at 286.5 eV (also detected in the O1s spectra at 533.6 eV in Figure S5 in the Supporting information) is mostly attributed to polymeric species, e.g., poly(ethylene oxide) (PEO),[3,12] generated upon the decomposition of the solvents. e.g., the polymerization reaction of EC initiated by strong nucleophilic species, such as alkoxide anions, reported below.[13]

$$n(CH_2O)_2CO \rightarrow (-CH_2-CH_2-O-)_n \downarrow + nCO_2 \uparrow$$

Among the lithiated graphite electrodes (Figure 4), the C–O–C contribution is slightly lower for the electrode subjected to the single-current protocol than for the other two. Furthermore, the Li_2O signal is found in the O1s spectra (ca. 528 eV in Figure S4 in the Supporting information) of such an electrode. In the case of single- and dual-current protocols a weak signal of lithiated graphite species Li_xC_6 and/or lithium carbide (Li_2C_2) is also detected at 282.4 eV.[3,13a] Carbonates (such as the stable Li_2CO_3 and the metastable alkyl lithium carbonates, $ROCO_2Li$) are found in all electrodes between 289.5 and 291 eV.[3,13a] The carbonates result from the EC and DMC decomposition reactions such as:[13a,c, 14]

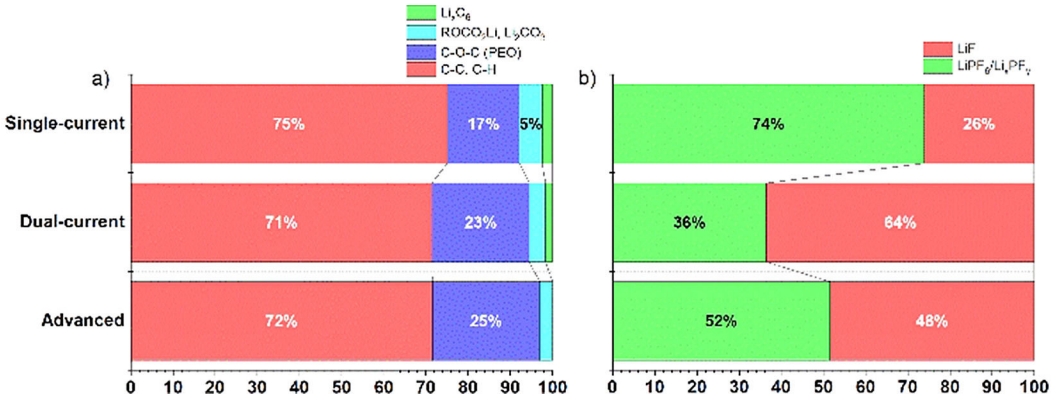

Figure 4. Percentage of the SEI compounds obtained from the deconvolution of the spectra in Figure 3.

$$(CH_2O)_2CO + 2e^- + 2Li^+ \rightarrow Li_2CO_3 \downarrow + C_2H_4 \uparrow$$

$$2CH_3OCO_2CH_3 + 2e^- + 2Li^+ \rightarrow 2CH_3OCO_2Li \downarrow + C_2H_6 \uparrow$$

or by the further decomposition at low potential (<400 mV) of the initially formed, organic SEI.[15]

Nevertheless, their amount is below 5% for both the dual-current and the advanced protocol. The electrodes subjected to these two protocols also show a substantially higher amounts of LiF (peak at 685.0 eV in Figure 3 d–f[3]) with respect to the single-current protocol. LiF is mainly originating from salt decomposition, initiated by water traces,[16] HF contamination[17] and/or FEC decomposition.[18]

It is interesting to note that although performed at different temperature (20 °C and 40 °C respectively), the dual-current and advanced protocols generate similar SEI compositions, with the main difference being about 20% more LiF for the former one.

2.3. HRTEM Investigation of the SEI Formed Using Different Formation Protocols

In order to follow the evolution of the SEI upon formation and cycling, TEM images of the graphite electrodes were taken on as made electrodes, after the formation cycle with the various protocols and after 100 charge/discharge cycles at 1 C. Figure 5

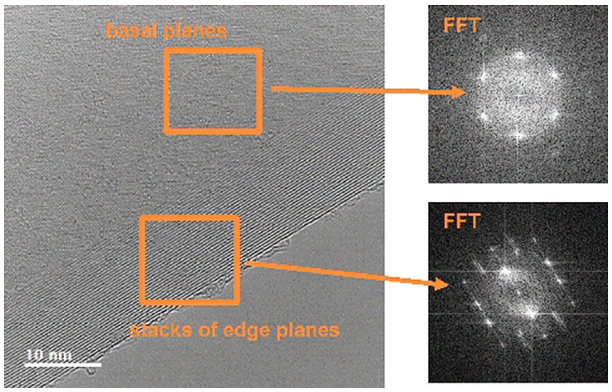

Figure 5. HRTEM image and the corresponding FFT images of the pristine graphite.

shows the HRTEM image of the pristine graphite material where both basal and edge graphite planes can be distinguished. The interplanar distance of the graphene sheets was determined to be ~3.67 Å.

The HRTEM images of the graphite particles subjected to the different formation protocols are shown in Figure 6. The figures report the boundary area between the basal and the edge planes of a graphite particle (a schematic representation of the inspected area is reported in Figure S6 in the Supporting Information). Despite the fact that, without a statistical evaluation, the images reported herein may not represent all graphite particles in the electrode, they give useful information

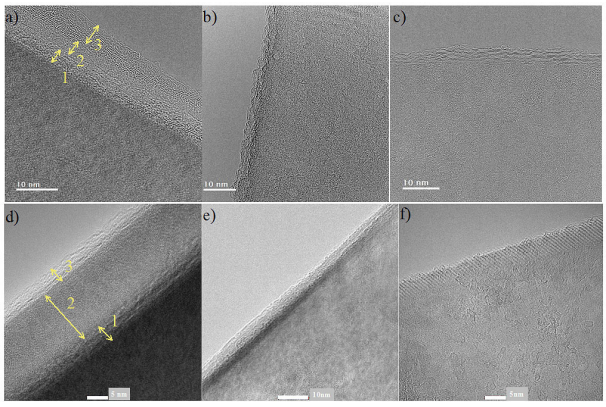

Figure 6. HRTEM images of graphite particles in the fully delithiated state after the formation (from a to c) and cycling at 1 C (from d to f) using the a,d) single-current, b,e) double-current and c,f) advanced formation protocol.

about the microscopic morphology of the investigated samples.

Normally, a thicker SEI is expected at the edges of graphite particles because of the higher reactivity of the edge carbon atoms with respect to those in the basal plane and the anisotropic nature of Li^+ insertion.[19] The single-current formation cycle (panel a) resulted in a pronounced amorphization of the edge planes as compared to the pristine material. The SEI formed using this protocol consists of three layers with different textures (marked with numbers "1", "2" and "3"). While in layers "1" and "3" the graphene sheets can still be distinguished, the layer "2" appears to be rather amorphous. With the dual-current protocol (panel b), the graphite amorphization upon formation is taking place. The graphene planes are barely distinguished in the single, rough, surface film formed whose thickness is, however, lower than that obtained with the single-current formation. On the other hand the surface of the graphite particles subjected to the advanced protocol (Figure 6c), appears much less disordered as the graphene layers at edge planes, although deformed, are still clearly visible.

Overall, the HRTEM investigation evidences that the graphene sheets near the edges amorphize upon cell formation independent on the protocol used, but to a rather different extent. This effect has been previously reported by Sethuraman et al.,[20] attributing this process to shallow Li intercalation generating a steep concentration gradient between the fully occupied surface layers near the plane edges and the graphite bulk resulting in lattice deformation. On the other hand, Tokranov et al.[21] attributed the amorphization of graphite surface to the insertion of solvated ions, occurring after the formation of passivating inorganic species (below 0.65 V) and before the threshold for Li intercalation (below 0.2 V). However, it is reasonable to consider that, most likely, the graphene sheet disordering is due to a combination of both factors. The results herein reported show that the amorphization is higher when the charge rate is lower, such as in the single-current protocol at C/20. The reduced disorder observed with the dual-current protocol indicates that the intercalation rate of C/10 is more appropriate to avoid the shallow Li intercalation. The minimal

amorphization detected for the advanced-protocol is the result of higher charging rate and temperature, both enabling the fast formation of the SEI.[8]

The progressive structural disordering of the graphite surface upon cycling has a negative impact on the SEI, inducing C–C bond breakage and exposing reactive sites to the electrolyte,[20] which consume Li^+ and thicken the SEI, thus reducing the cell capacity and cycle life.[20,22] This is confirmed by the HRTEM images taken after 100 cycles. For the single-current protocol, after cycling (Figure 6d) the thickness of the layer "2" substantially increases, indicating the growth of the SEI. At the same time, further amorphization of the graphite sheets in layers "1" and "3" is observed. In the case of dual-current (Figure 6e), the layer completely amorphizes and smoothens while its slight thickness increase occurs (although confined with respect to the single-current protocol). Instead no major surface changes are detected after 100 cycles on the graphite electrode subjected to the advanced protocol (Figure 6d).

The most accepted model describes the SEI as multiple layer on top of the edge planes of graphite particles.[9,23] However, the HRTEM images harvested from the samples after the formation cycle do not reveal any clear additional surface film but rather SEI species intercalated in between disordered graphene sheets, matching well with the early study of Besenhard et al..[24] These authors suggested that the electrolyte decomposition products form in between the layers and, thus, the SEI film penetrates the graphite surface. This observation would also explain the detection of Li_xC_6 and/or carbide Li_2C_2 signal at 282.4 eV in the C1s XPS spectra for the single- and dual-current protocols (Figure 3 a,b). However, in the case of the single-current protocol, after 100 cycles the graphite surface appears to be covered by rounded shaped amorphous particles as shown in Figure 7. Figure 8 reports the HRTEM images of the

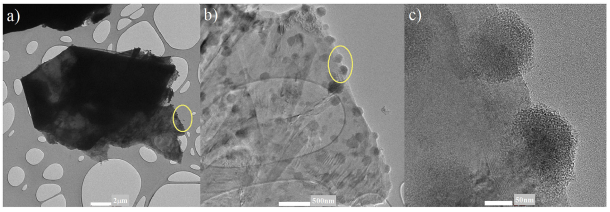

Figure 7. HTREM images at different magnification obtained from the same samples reported in Figure 6d (single-current formation). The yellow circles highlight the area magnified in the subsequent panel.

cycled graphite electrodes subjected to the dual-current formation (see also Figure 6e) and the advanced formation (see also Figure 6f). In both cases only very small and sporadic deposits are detected, reflecting the importance of reducing the initial amorphization to minimize the electrolyte consumption upon cycling.

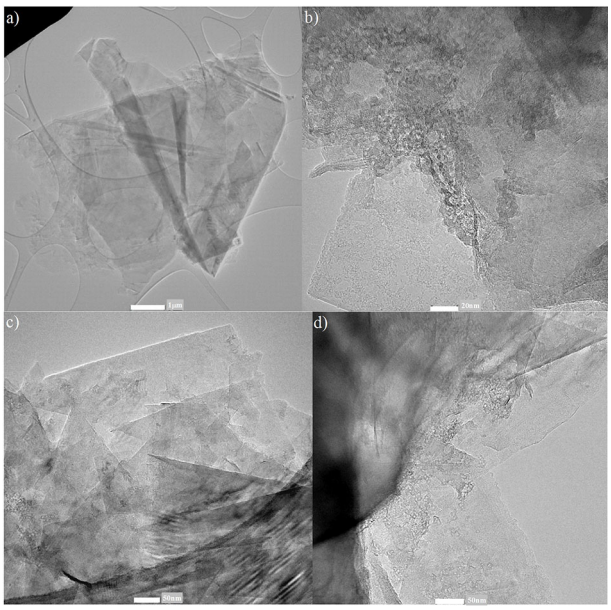

Figure 8. HRTEM images at different magnification obtained from the same samples reported in Figure 6. Graphite extracted after prolonged cycling after the dual-current formation protocol (a and b) and advanced protocol (c and d).

3. Conclusions

Aiming to reduce the formation time, the influence of three different charging protocols on the graphite//LFP cell performance and the anodes SEI characteristics was investigated. Independently of the formation protocol, satisfactory cycling performance in lab-scale graphite//LFP coin cells are obtained. The temperature employed in the first charge, seems not to strongly affect the SEI composition. Indeed, although conducted at 40 °C, the SEI formed with the advanced protocol has similar composition to that obtained at 20 °C using the dual-current protocol. The main difference resides in the LiF content, higher for the dual-current protocol then for all the others. On the other hand, the charge rate directly impacts the grade of amorphization of graphite surface generating a thick SEI for the single-current protocol and minimal modifications for the advanced. The dual-current, instead, results in an intermediate level of graphite surface disorder and moderate SEI growth upon cycling. Overall the dual-current appears to be a suitable protocol for our graphite//LFP cells as results in stable cycling performance, limited graphite surface amorphization and in an SEI enriched with stable and protective LiF.[25] Furthermore, the dual-current protocol permits to reduce remarkably the formation time while simultaneously enabling satisfactory electrochemical performance. It is important to remark that, due to the dependence of the SEI's final characteristics not only on the formation conditions, but also on the electrode surface and electrolyte composition, a formation protocol should be always further optimized and validated whenever a change in the cell chemistry takes place.

Experimental Section

Electrodes and Electrolytes

The calendered graphite (SLP30, Timcal) and $LiFePO_4$ (LFP, Prayon) electrodes were manufactured at CEA-LITEN. The graphite electrodes, comprising 96% wt. of active material and made via aqueous process using commercial high viscosity CMC and SBR as binders (2%wt. of each respectively), were calendered to a porosity of 39%, and had an average loading of ca. 8 mg cm^{-2} (~2.5 mAh cm^{-2}). The LFP electrodes with 90.5% wt. of active material, 5%wt. carbon black (Imerys C65), 4.5%wt, polyvinylidene difluoride binder (Solvay, Solef®5130) and 35% porosity (made using conventional organic solvent-based slurry) had an average loading of 17.5 mg cm^{-2} (~2.3 mAh cm^{-2}), determining an anode/cathode capacity ratio of 1.1 for the graphite/LFP Li-ion cells. The electrodes were dried under vacuum at 120 °C for 6 h prior the transfer in argon filled glove-box for cell assembly (O_2 and H_2O levels below 0.1 ppm).The electrolyte was prepared by adding 2 wt.% of FEC additive (UBE, Japan) into 1 M $LiPF_6$ in ethylene carbonate (EC) : dimethyl carbonate (DMC) (1:1, v/v) electrolyte (UBE, Japan) and mixing the mixture for 12 h in an argon-filled glove-box.

Electrochemical Tests

Coin cells (type 2032) were assembled in an argon filled glove-box by sandwiching a glass fiber separator (Whatman GF/D) soaked with 100 μL of electrolyte between graphite and LFP electrodes (1.13 cm^2). The three formation protocols are described in Table 1. The charge always included a constant voltage (CV) step at the upper cut-off voltage. All cells were subjected to a rest period of 24 h at 20 °C prior formation to ensure complete electrode wetting. The cycling rate of 1 C is calculated based on theoretical capacity of the cathode material (170 mAhg^{-1}) and the active material loading. After the formation cycle the cells (three for each protocol under investigation), performed a rate test and, afterward, were let to cycle at 1 C. The detailed cycling protocol is reported in Table S1 in the Supporting information.

X-Ray Photoelectron Spectroscopy (XPS)

To analyze the variation of graphite's SEI composition with the three formation protocols, graphite/LFP cells were disassembled in the glove-box after being charged. The extracted graphite electrodes were carefully rinsed with 200 μL of DMC and dried under vacuum for 30 min. The electrodes were then placed in an airtight vessel and transferred to the XPS sample chamber. The measurements were performed using a PHI 5800 MultiTechnique ESCA System with monochromatized Al–Kα (1486.6 eV) radiation. The detection angle of the measurement was 45° and pass energies of 93.9 and 29.35 eV were used for survey and detailed spectra, respectively. The binding energies were calibrated to the C1s signal of graphite at 284.6 eV and analyzed using CasaXPS software. In order to directly compare the different samples, the peaks' area were normalized to the sum of the peaks areas detected for the electrode subjected to the single-current formation protocol.

High-Resolution Transmission Electron Microscopy (HRTEM)

The graphite electrodes (in de-lithiated state) were extracted from graphite/LFP coin cells after the 1st formation cycle and 104 cycles (see Table S2 in the Supporting information). As for the XPS samples, the cells were disassembled in the glove-box and the harvested electrodes were rinsed with 200 μL of DMC and dried in vacuum for 30 min. Graphite powder samples were scratched from the current collector, gently ground in an agate mortar before being deposited over the TEM grid without using any solvent. The grids were then transferred to the microscope using an airtight sample holder. High-resolution images were recorded using a FEI Titan Themis microscope running in TEM mode and operated at 200 kV.

Acknowledgements

The authors acknowledge the financial support from the EU under the grant agreement no. 653373 (SPICY – Silicon and polyanionic chemistries and architectures of Li-ion cell for high energy battery, H2020-GV-2014). Dr. Thomas Diemant (University of Ulm) is kindly acknowledged for the XPS measurements.

Conflict of Interest

The authors declare no conflict of interest.

Keywords: charging protocols · electron microscopy · graphite · lithium-ion batteries · SEI formation

[1] E. Peled, *J. Electrochem. Soc.* **1979**, *126*, 2047–2051.
[2] S. J. An, J. Li, C. Daniel, D. Mohanty, S. Nagpure, D. L. Wood Iii, *Carbon* **2016**, *105*, 52–76.
[3] P. Verma, P. Maire, P. Novák, *Electrochim. Acta* **2010**, *55*, 6332–6341.
[4] D. L. Wood Iii, J. Li, C. Daniel, *J. Power Sources* **2015**, *275*, 234–242.
[5] S. J. An, J. Li, Z. Du, C. Daniel, D. L. Wood, *J. Power Sources* **2017**, *342*, 846–852.
[6] P.-C. J. Chiang, M.-S. Wu, J.-C. Lin, *Electrochem. Solid-State Lett.* **2005**, *8*, A423–A427.
[7] a) J. Li, E. Murphy, J. Winnick, P. A. Kohl, *J. Power Sources* **2001**, *102*, 302–309; b) B. K. Antonopoulos, C. Stock, F. Maglia, H. E. Hoster, *Electrochim. Acta* **2018**, *269*, 331–339; c) F.-M. Wang, H.-Y. Wang, M.-H. Yu, Y.-J. Hsiao, Y. Tsai, *J. Power Sources* **2011**, *196*, 10395–10400.
[8] C. Huang, K. Huang, H. Wang, S. Liu, Y. Zeng, *J. Solid State Electrochem.* **2011**, *15*, 1987–1995.
[9] S. J. An, J. Li, Z. Du, C. Daniel, D. L. Wood Iii, *J. Power Sources* **2017**, *342*, 846–852.
[10] S. J. An, J. Li, C. Daniel, D. Mohanty, S. Nagpure, D. L. Wood, *Carbon* **2016**, *105*, 52–76.
[11] B. R. Long, S. G. Rinaldo, K. G. Gallagher, D. W. Dees, S. E. Trask, B. J. Polzin, A. N. Jansen, D. P. Abraham, I. Bloom, J. Bareño, J. R. Croy, *J. Electrochem. Soc.* **2016**, *163*, A2999–A3009.
[12] a) R. Dedryvère, S. Leroy, H. Martinez, F. Blanchard, D. Lemordant, D. Gonbeau, *J. Phys. Chem. B* **2006**, *110*, 12986–12992; b) D. Ensling, M. Stjerndahl, A. Nyten, T. Gustafsson, J. O. Thomas, *J. Mater. Chem.* **2009**, *19*, 82–88; c) C. M. Ghimbeu, C. Decaux, P. Brender, M. Dahbi, D. Lemordant, E. Raymundo-Piñero, M. Anouti, F. Béguin, C. Vix-Guterl, *J. Electrochem. Soc.* **2013**, *160*, A1907–A1915; d) H. Kim, S. Grugeon, G. Gachot, M. Armand, L. Sannier, S. Laruelle, *Electrochim. Acta* **2014**, *136*, 157–165.
[13] a) G. G. Eshetu, T. Diemant, S. Grugeon, R. J. Behm, S. Laruelle, M. Armand, S. Passerini, *ACS Appl. Mater. Interfaces* **2016**, *8*, 16087–16100; b) G. Gachot, S. Grugeon, M. Armand, S. Pilard, P. Guenot, J.-M. Tarascon, S. Laruelle, *J. Power Sources* **2008**, *178*, 409–421; c) S. Leroy, H. Martinez, R. Dedryvère, D. Lemordant, D. Gonbeau, *Appl. Surf. Sci.* **2007**, *253*, 4895–4905.
[14] R. Dedryvère, H. Martinez, S. Leroy, D. Lemordant, F. Bonhomme, P. Biensan, D. Gonbeau, *J. Power Sources* **2007**, *174*, 462–468.
[15] B. K. Antonopoulos, F. Maglia, F. Schmidt-Stein, J. P. Schmidt, H. E. Hoster, *Batteries & Supercaps* **2018**, *1*, 110–121; Supercaps **2018**, 1, 110–121.

[16] T. Kawamura, A. Kimura, M. Egashira, S. Okada, J.-I. Yamaki, *J. Power Sources* **2002**, *104*, 260–264.
[17] D. Strmcnik, I. E. Castelli, J. G. Connell, D. Haering, M. Zorko, P. Martins, P. P. Lopes, B. Genorio, T. Østergaard, H. A. Gasteiger, F. Maglia, B. K. Antonopoulos, V. R. Stamenkovic, J. Rossmeisl, N. M. Markovic, *Nat. Catal.* **2018**, *1*, 255–262.
[18] a) M. Nie, J. Demeaux, B. T. Young, D. R. Heskett, Y. Chen, A. Bose, J. C. Woicik, B. L. Lucht, *J. Electrochem. Soc.* **2015**, *162*, A7008–A7014; b) V. Etacheri, O. Haik, Y. Goffer, G. A. Roberts, I. C. Stefan, R. Fasching, D. Aurbach, *Langmuir* **2012**, *28*, 965–976.
[19] E. Peled, S. Menkin, *J. Electrochem. Soc.* **2017**, *164*, A1703–A1719.
[20] V. A. Sethuraman, L. J. Hardwick, V. Srinivasan, R. Kostecki, *J. Power Sources* **2010**, *195*, 3655–3660.
[21] A. Tokranov, B. W. Sheldon, P. Lu, X. Xiao, A. Mukhopadhyay, *J. Electrochem. Soc.* **2014**, *161*, A58–A65.
[22] N. Susarla, S. Ahmed, D. W. Dees, *J. Power Sources* **2018**, *378*, 660–670.
[23] a) K. Edström, M. Herstedt, D. P. Abraham, *J. Power Sources* **2006**, *153*, 380–384; b) E. Peled, D. Golodnitsky, G. Ardel, *J. Electrochem. Soc.* **1997**, *144*, L208–L210.
[24] J. O. Besenhard, M. Winter, J. Yang, W. Biberacher, *J. Power Sources* **1995**, *54*, 228–231.
[25] a) Q. Zhang, J. Pan, P. Lu, Z. Liu, M. W. Verbrugge, B. W. Sheldon, Y.-T. Cheng, Y. Qi, X. Xiao, *Nano Lett.* **2016**, *16*, 2011–2016; b) V. Sharova, A. Moretti, T. Diemant, A. Varzi, R. J. Behm, S. Passerini, *J. Power Sources* **2018**, *375*, 43–52.

Manuscript received: October 19, 2018
Revised manuscript received: December 11, 2018
Version of record online: January 18, 2019